Iranian Journal of Materials Science and Engineering, Vol. 20, Number 4, December 2023
RESEARCH PAPER

Johnson–Mehl–Avrami–Kolmogorov (JMAK-type) Analysis of Deformation-Induced Martensitic Transformation in AISI 304L Stainless Steel

Mohammad Javad Sohrabi[1], Hamed Mirzadeh[1,*], Saeed Sadeghpour[2], Reza Mahmudi[1]

* *hmirzadeh@ut.ac.ir*

[1] School of Metallurgy and Materials Engineering, College of Engineering, University of Tehran, Tehran, Iran
[2] Centre for Advanced Steels Research, Materials and Mechanical Engineering, University of Oulu, 90014 Oulu, Finland

Received: August 2023 **Revised: October 2023** **Accepted: October 2023**
DOI: 10.22068/ijmse.3335

Abstract: *Deformation-induced α′-martensite generally forms at shear bands in the coarse-grained austenite, while it nucleates at grain boundaries in the ultrafine-grained (UFG) austenite. The available kinetics models are related to the nucleation on the shear band intersections. Hence, their application to investigating the kinetics of α′-martensite formation for the UFG regime cannot be justified. Accordingly, in the present work, the general Johnson–Mehl–Avrami–Kolmogorov (JMAK-type) model was implemented for comparing the kinetics of α′-martensite formation in the UFG and coarse-grained regimes using an AISI 304L stainless steel. On the experimental front, the X-ray diffraction (XRD) patterns and the electron backscattered diffraction (EBSD) maps were used for phase and microstructural analyses, respectively. It was revealed that the simple JMAK-type model, by considering the dependency of the volume fraction of α′-martensite on the strain, is useful for modelling the experimental data, predicting the nucleation sites based on the theoretical Avrami exponents, and characterizing the transformation kinetics at low and high strains.*

Keywords: *Metastable austenitic stainless steels, Grain size, Transformation-induced plasticity, Kinetics of phase transformations, Johnson–Mehl–Avrami–Kolmogorov model.*

1. INTRODUCTION

During the deformation of metastable austenitic stainless steels, the deformation-induced α′-martensite formation significantly increases the work-hardening rate [1, 2] and leads to retardation of necking toward enhanced ductility, which is known as the transformation-induced plasticity (TRIP) effect [3-5]. This phase transformation depends on austenite stability. Since the formation of stacking faults and related features are the perquisites for deformation-induced α′-martensite formation, the increase in the stacking fault energy (γ_{SFE}) usually leads to an increase in the austenite stability against α′-martensite formation. Commonly, low γ_{SFE} favours martensitic transformation an increase in γ_{SFE} promotes mechanical twinning, and high γ_{SFE} leads to slipping [4]. The γ_{SFE} depends on material parameters, such as chemical composition and grain size [6-8], and deformation conditions such as deformation temperature [9-11].

Due to its effect of increasing the apparent stacking fault energy (γ_{SFE}), grain refinement increases the austenite stability against α′-martensite formation and suppresses the TRIP effect [7, 8]. However, recent results showed that this trend is not followed in the ultrafine-grained (UFG) regime, in which the kinetics of martensite formation is unusually high. In this case, the nucleation of α′-martensite occurs at grain boundaries instead of the shear band intersections (e.g., ε-martensite) in the coarse-grained regime [8, 12, 13]. Therefore, it is expected that the kinetics of α′-martensite formation is different for the UFG and coarse-grained regimes, which needs to be characterized in a systematic study.

Regarding the kinetics of the deformation-induced martensitic transformation, many models have been developed [14-20]. In this respect, Olson and Cohen [15] proposed the most widely used model by introducing two parameters of α and β, where the former depicts the rate of the shear band formation and the latter is related to the probability that α'-martensite is nucleated at a shear band intersection. To obtain a better fit, several modifications of this model have also been proposed [14, 18-20]. The Olson-Cohen model and its derivatives are related to the nucleation on the shear bands. Hence, their application for investigating the kinetics of α′-martensite formation for the UFG regime

[DOI: 10.22068/ijmse.3335]

cannot be justified. Accordingly, a general model should be utilized for this purpose.
The Johnson–Mehl–Avrami–Kolmogorov (JMAK-type) model is generally used for investigating phase transformation. Accordingly, it is logical to implement it for comparing the kinetics of α′-martensite formation for the UFG and coarse-grained regimes. Therefore, the present work is dedicated to the JMAK-type analysis of deformation-induced martensitic transformation in the metastable AISI 304L stainless steel for both UFG and coarse-grained regimes.

2. EXPERIMENTAL PROCEDURES

Thermomechanical processing of cold rolling and reversion/recrystallization/grain growth annealing was used to process an AISI 304L stainless steel with the chemical composition shown in Table 1. As shown in Figure 1, the sheets were 80% cold rolled, followed by isothermal annealing at 850 and 1000°C for various holding times. Accordingly, sheets with average grain sizes of 0.5, 2.7, 5.6, and 34 µm were obtained by annealing at 850°C for 3 min, 850°C for 5 min, 850°C for 15 min, and 1000°C for 30 min, respectively. Then, the room-temperature rolling with the percent reduction in thickness (r) in the range of 12.5% to 87.5% was used to induce the formation of different volume fractions of the α′-martensite ($f_{a'}$) from austenite (γ). More details can be found elsewhere [7, 21]. The constancy of volume during plastic deformation leads to $\varepsilon_{longitudinal} + \varepsilon_{thickness} + \varepsilon_{width} = 0$, where the plane-strain rolling, and hence, the von Mises equivalent strain can be presented as $\varepsilon_{Rolling} = \sqrt{(2/3)(\varepsilon^2_{longitudinal} + \varepsilon^2_{thickness} + \varepsilon^2_{width})}$.

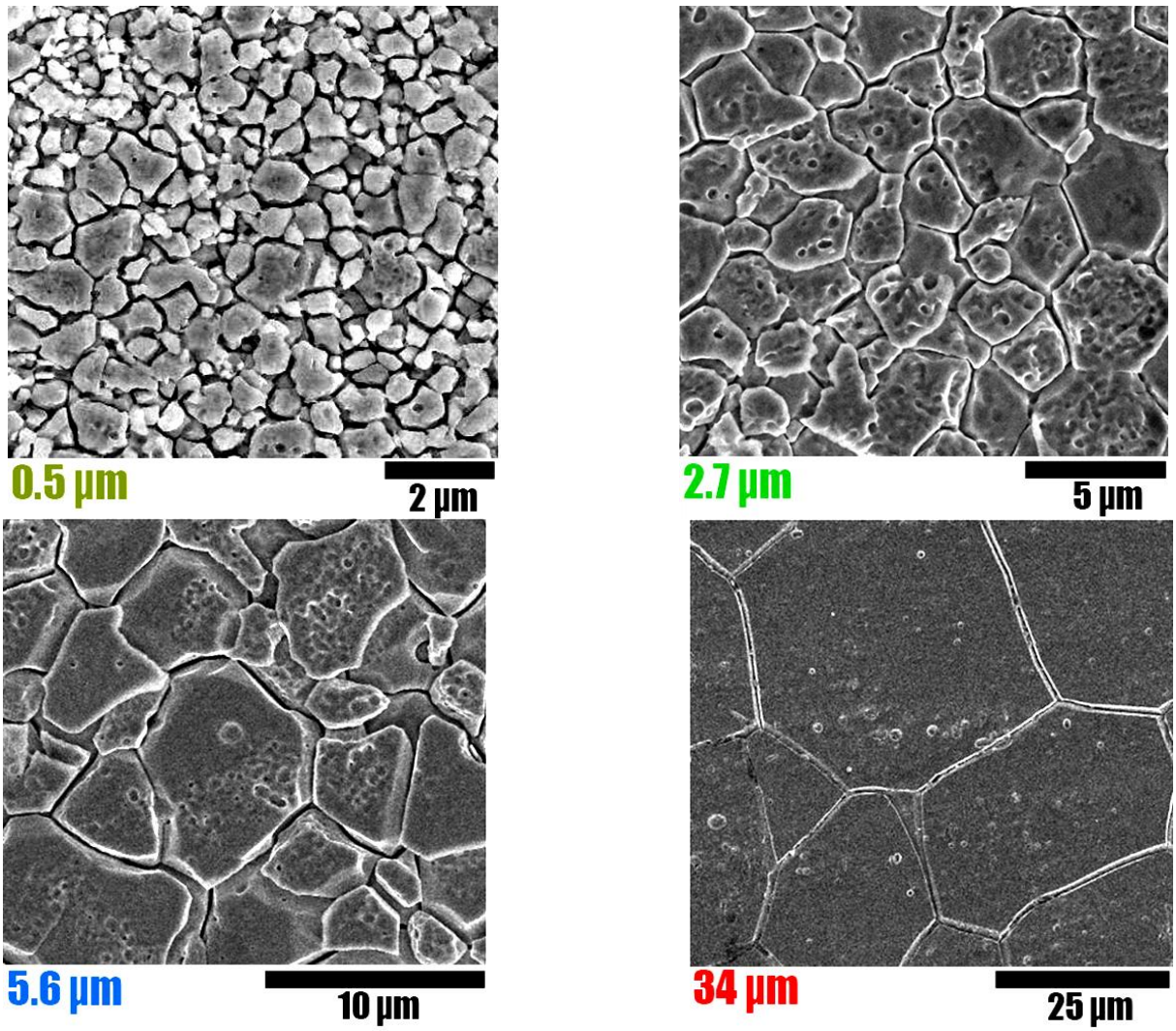

Fig. 1. FESEM images of AISI 304L samples with different grain sizes of 0.5, 2.7, 5.6, and 34 µm.

[DOI: 10.22068/ijmse.3335]

Since $\varepsilon_{thickness} = \ln(1/(1-r))$, the equation of $\varepsilon_{Rolling} = 1.1547\ln(1/(1-r))$, is obtained. Accordingly, r in the range of 12.5% to 87.5% is equivalent to $\varepsilon_{Rolling}$ in the range of 0.15 to 2.4. Electro-etching (60% HNO_3 solution at 2 V) preceded by the electro-polishing (H_3PO_4-H_2SO_4 solution at 40 V) was used to reveal the microstructures using a field emission scanning electron microscope (FESEM); while electro-polishing with the perchloric acid solution was used to prepare samples for detailed microstructural investigation using a Zeiss Sigma FESEM equipped with an electron backscattered diffraction (EBSD) detector operating under an accelerating voltage of 15 kV and step size of 0.05-0.2 µm. A PHILIPS PW-3710 X-ray diffractometer (XRD) with Cu-Kα radiation was used to calculate $f_{a'}$ using Equation 1 [22], which is a semi-empirical relationship that has been developed and well-accepted for the quantification of the α′-martensite phase in austenitic stainless steel and considers the intensities of γ(220) and γ(311) for austenite and that of α′(211) for α′-martensite:

$$f_{a'} = I_{(211)a'}/\{I_{(211)a'} + 0.65(I_{(311)\gamma} + I_{(220)\gamma})\} \quad (1)$$

Table 1. Chemical composition (wt.%) of AISI 304L stainless steel

C	Cr	Ni	Mn	Mo	Fe
0.01	18.6	8.3	1.4	0.1	**Balance**

3. RESULTS AND DISCUSSION

Room-temperature rolling with *r* in the range of 12.5 to 87.5% was used to obtain different $f_{a'}$, where the corresponding XRD patterns are depicted in Figure 2. It can be seen that by increasing *r*, the intensity of the characteristic austenite peak decreases, while those for the α′-martensite increase. This reveals that $f_{a'}$ increases with increasing *r*. The values of $f_{a'}$ were calculated by Equation 1, and the results are summarized in Figure 3.

Figure 3 reveals that the curves of $f_{a'}$ versus $\varepsilon_{Rolling}$ have a sigmoidal shape, which is a general expectation for phase transformations and phenomena such as recrystallization for engineering materials [23-25]. Therefore, the JMAK-type analysis can be applied by substituting time with $\varepsilon_{Rolling}$:

$$f_{a'} = 1 - \exp(-K\varepsilon_{Rolling}^{n}) \quad (2)$$

Where n is the Avrami exponent [26-28] and is associated with the nucleation mode; while K is associated with the nucleation and growth rates. Based on Equation 2, the equation of $\ln\{1-f_{a'}\} = -k\varepsilon_{Rolling}^{n}$ can be obtained, and hence, the relationship of $\ln[\ln\{1/(1-f_{a'})\}] = \ln K + n\ln\varepsilon_{Rolling}$ is resulted. Accordingly, as shown in Figure 4, the slope and the intercept of the plot of $\ln[\ln\{1/(1-f_{a'})\}]$ versus $\ln\varepsilon_{Rolling}$ give n and ln K, respectively. The obtained regression results are also indicated in the figure.

Figure 4 shows that the data for each grain size follows a straight line, which reveals that the JMAK-type analysis can be adequately applied to represent the γ to α′-martensite transformation in this material.

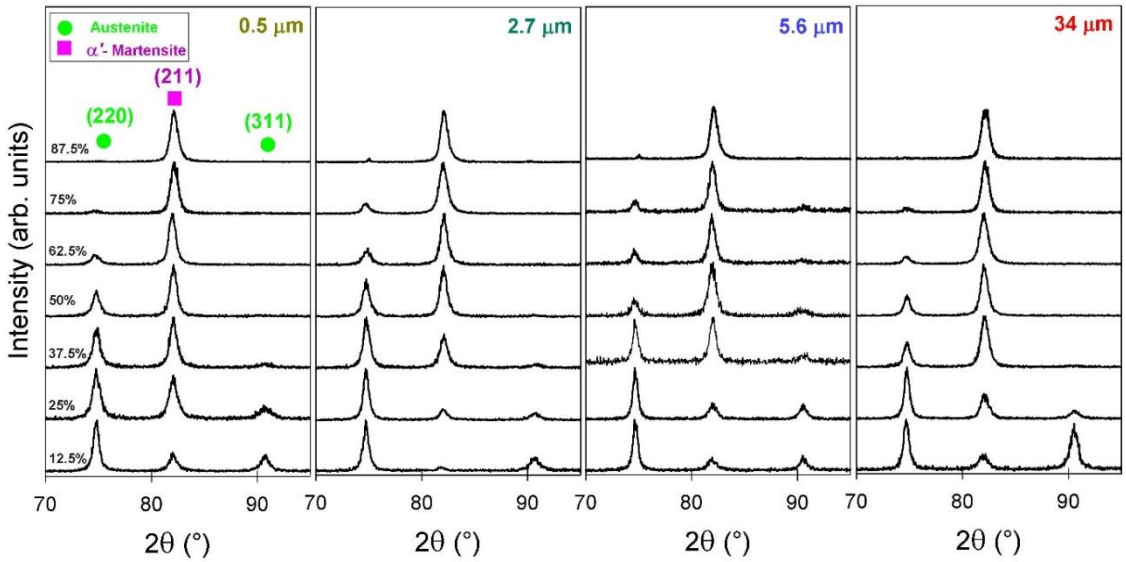

Fig. 2. XRD patterns of cold rolled AISI 304L samples with different grain sizes of 0.5, 2.7, 5.6, and 34 µm.

[DOI: 10.22068/ijmse.3335]

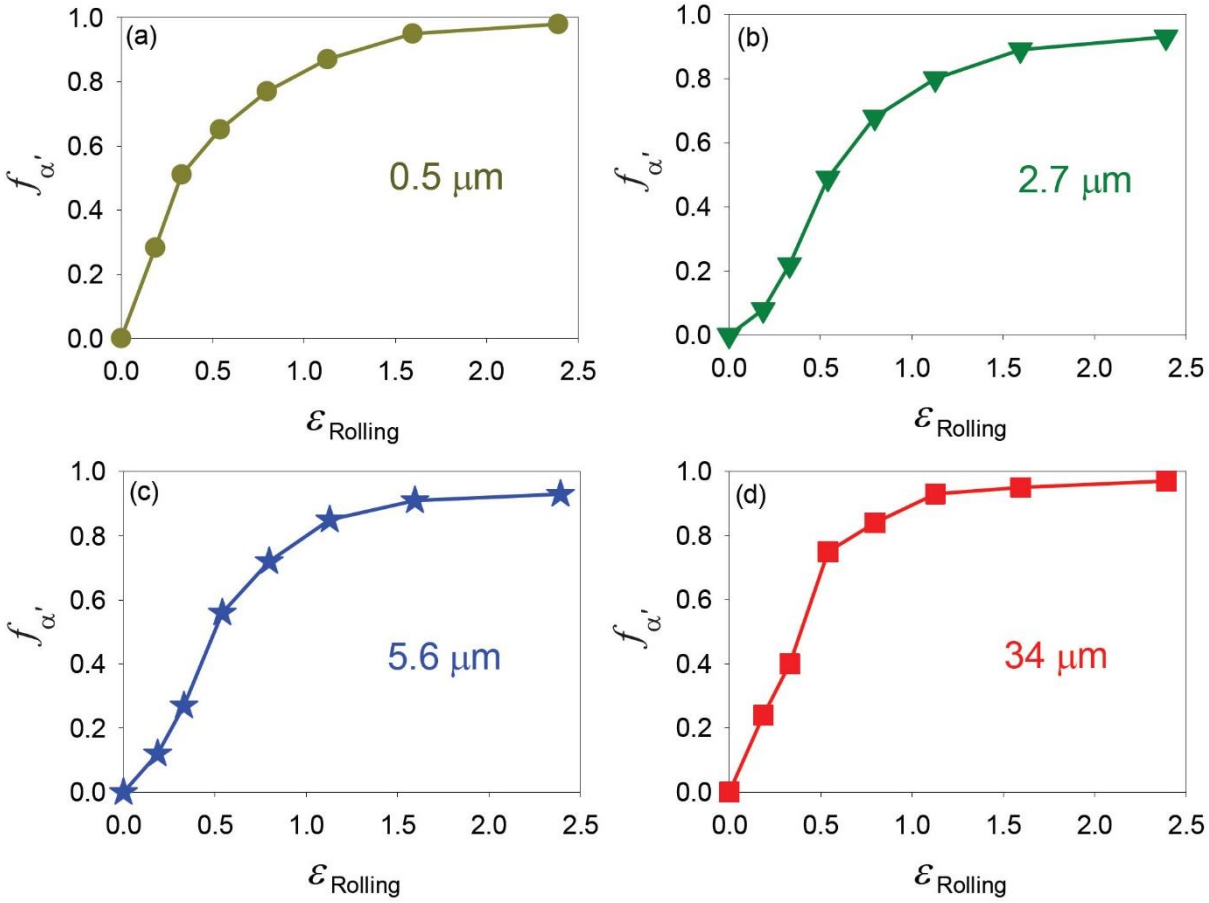

Fig. 3. Dependency of the martensite content on the cold rolling equivalent strain for different grain sizes of 0.5, 2.7, 5.6, and 34 μm.

It can be seen that the Avrami exponent (n) is ~1 for the grain size of 0.5 μm (UFG regime); while it is higher for the grain sizes of 2.7, 5.6, and 34 μm, where it can be taken as 1.6 on average for the coarse-grained regime.

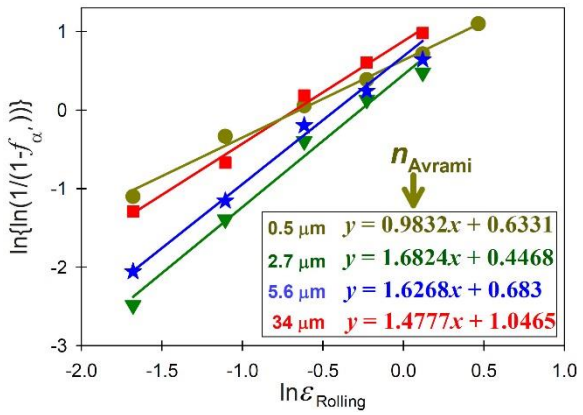

Fig. 4. JMAK-type plots for the cold rolled AISI 304L stainless steel with different grain sizes.

The difference in the slope of the line related to 0.5 μm with those of the other lines is also evident in Figure 4. The n value of ~1 is known as nucleation on grain boundaries for different phase transformations and/or recrystallization [29, 30]. Therefore, it is important to investigate the nucleation site of α'-martensite, which is possible at low rolling strains (low $\varepsilon_{Rolling}$). Therefore, $r \approx$ 12.5% was considered for EBSD analysis for two grain sizes of 0.5 and 34 μm, as shown in Figure 5. It can be seen that the α'-martensite (regions with BCC crystal structure [4] as detected by EBSD) has nucleated on the grain boundaries for the grain size of 0.5 μm, while it is nucleated on the intragranular shear bands (e.g. ε-martensite, regions with HCP crystal structure [6] as detected by EBSD) in the case of 34 μm. These features are formed in the interior of the grains at the initial stages of plastic deformation, similar to other investigations [12, 13, 21]. The sequence of γ to α'-martensite, and γ to ε-martensite to α'-martensite can be seen for the grain sizes of 0.5 and 34 μm, respectively. This can be related to the

[DOI: 10.22068/ijmse.3335]

effect of decreasing grain size on the increment of the apparent stacking fault energy, which retards the formation of shear bands. Accordingly, the ε-martensite might not be formed in the fine-grained sample due to the difficulty of shear band formation. Conversely, due to the presence of a high density of grain boundaries, direct nucleation of α′-martensite on the grain boundaries of γ might become the major transformation sequence in this case [10, 12, 13]. It can be seen that the simple JMAK-type analysis can identify the nucleation site of α′-martensite in the present work, where the *n* value of ~1 is consistent with the microstructural analysis. It is also interesting to assess its applicability by consideration of data reported in other relevant works. For instance, Kisko *et al.* [12] investigated the formation of α′-martensite in austenitic low-Ni Cr–Mn stainless steel type 204Cu during tensile deformation, as shown in Figure 6a.

These authors reported the nucleation of α′-martensite mainly at grain boundaries for the UFG steel, while its nucleation at shear bands (sometimes via ε-martensite) for the coarse-grained steels. Now, the data reported in Figure 6a can be further analyzed. For tensile deformation, the von Mises equivalent strain ($\varepsilon_{Tensile}$) is equal to $\varepsilon_{longitudinal}$. Moreover, the equation can be used to obtain $\varepsilon_{Tensile}$ by consideration of the engineering strain ($e_{Tensile}$).

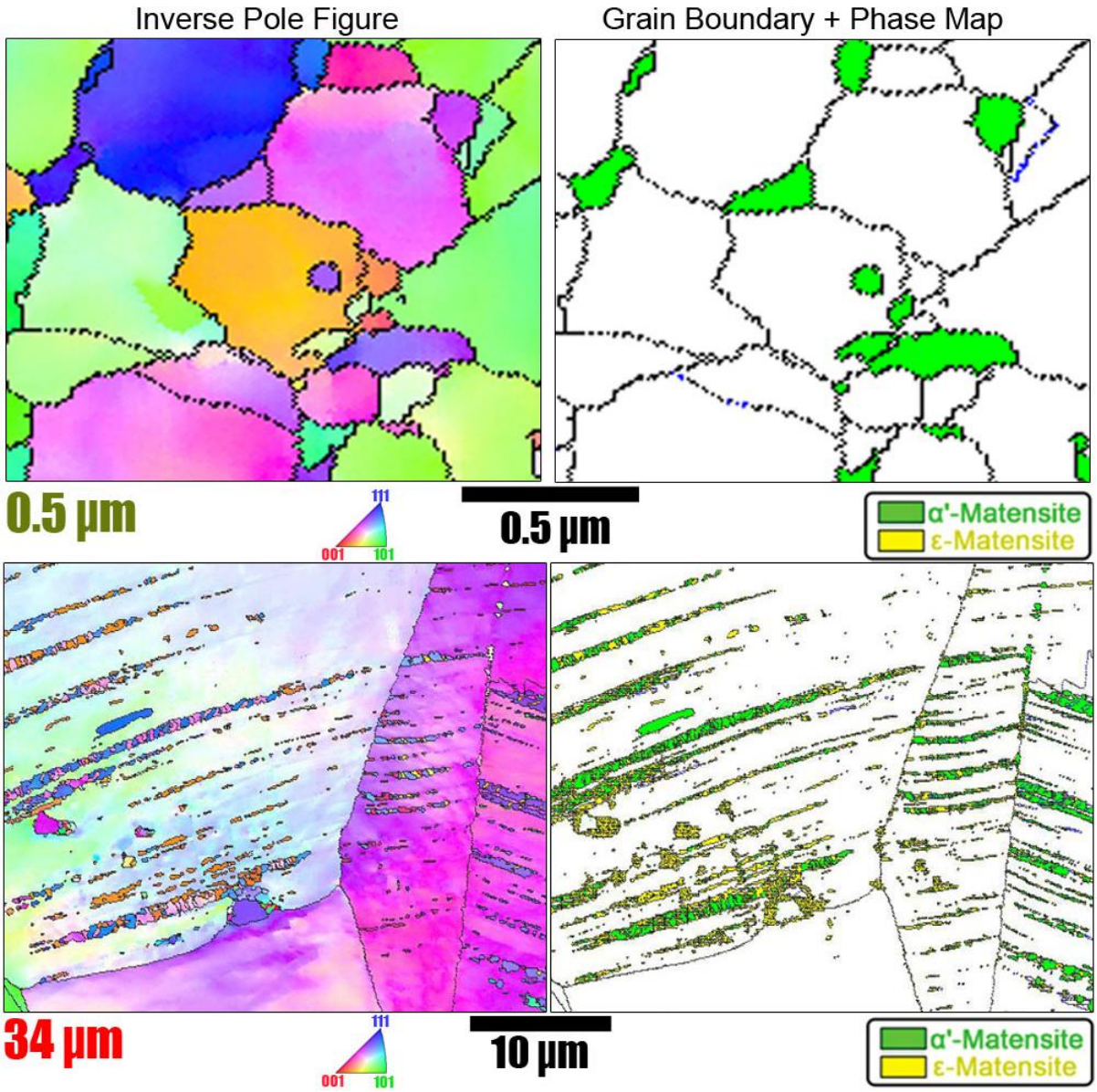

Fig. 5. EBSD maps of the 12.5% cold rolled AISI 304L stainless steel with two grain sizes of 0.5 and 34 µm.

[DOI: 10.22068/ijmse.3335]

Therefore, the data presented in Figure 6a can be used to obtain Figure 6b, where the *n* value of ~1 is seen for the UFG regime (grain size of 0.5 μm) but higher values (again ~ 1.6) are observed for coarser grain sizes.

These results confirm the applicability of the JMAK-type analysis for this purpose.

Kisko *et al.* [12] also observed that the transformation rate of strain-induced α'-martensite decreased with decreasing grain size; while the ultrafine grains transformed quite rapidly to martensite. This latter observation can be related to the presence of abundant nucleation sites in the microstructure of the UFG steel [12, 13, 21]. This effect has been investigated for the AISI 304L stainless steel in the present work, as depicted in Figure 7a. It can be seen that the transformation rate is higher for the sample with a grain size of 0.5 μm at low strains; while at large strains, the transformation rate for the sample with a grain size of 34 μm is higher. The former is related to the presence of a high density of grain boundaries as the nucleation sites (Figure 5, where the nucleation on the grain boundaries of the UFG stainless steel has been recently shown in several investigations [12, 13, 21]); while the latter can be ascribed to the formation of shear bands in the sample with a grain size of 34 μm at low strains, which are potent nucleation sites for the formation of α'-martensite at higher strains (Figure 5).

The results of Figure 7a can be further confirmed by considering the *n* value. It was discussed in Figure 4 that the UFG sample results in an *n* value of ~1 but other samples lead to a value of ~1.6. The effect of *n* is schematically shown in Figure 7b, where it can be seen that by increasing n (grain coarsening), the transformation rate at low strains decreases but it increases at large strains. These findings confirm that the transformation rate of austenite to α'-martensite for the UFG sample is different. To provide further evidence on the quantitative front, the obtained values of lnK are summarized in Figure 8.

It can be seen that the UFG sample (0.5 μm) does not follow the general trend seen for the coarser grains, and its K value is surprisingly high, which may be related to the nucleation on the grain boundaries in the UFG structure and fast growth.

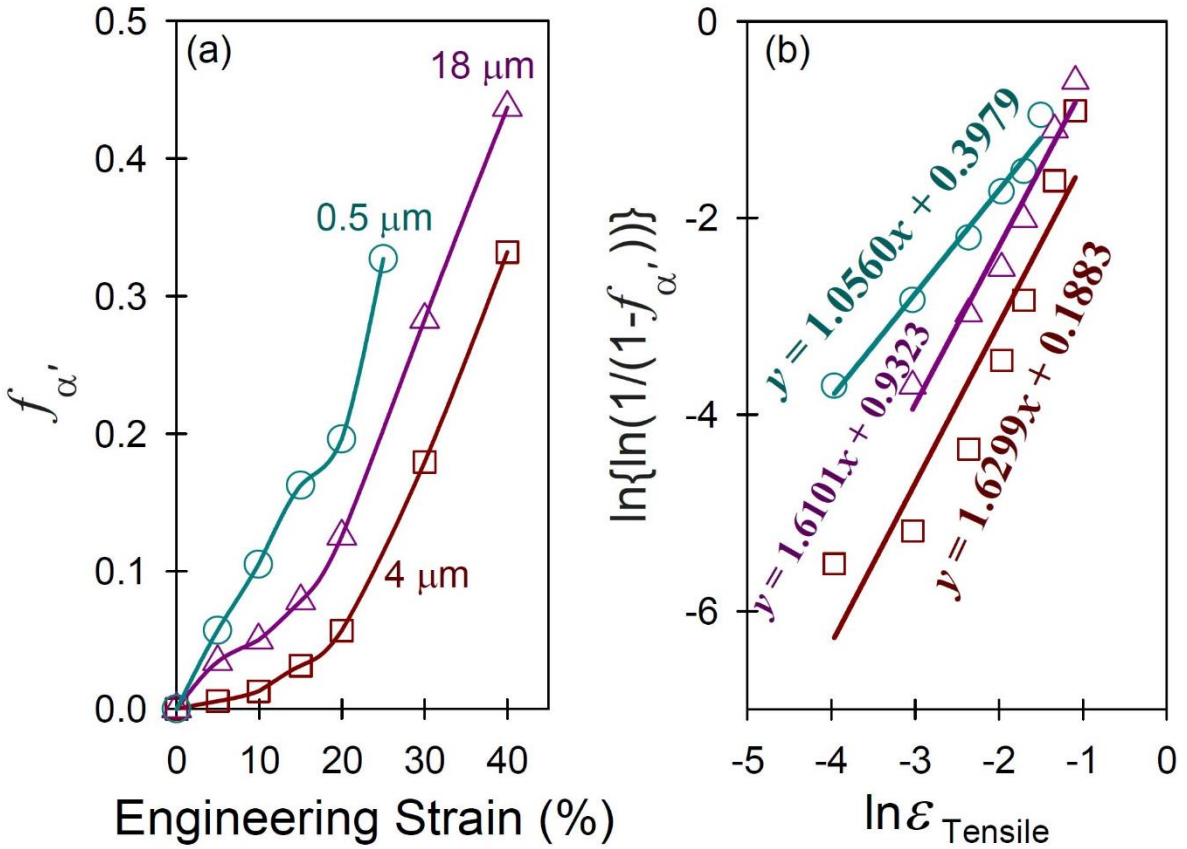

Fig. 6. (a) Variation of α' -martensite content with tensile strain for the austenitic low-Ni Cr-Mn stainless steel type 204Cu [12] and (b) the corresponding JMAK-type plots.

[DOI: 10.22068/ijmse.3335]

It is logical that the difference in the nucleation site also leads to a difference in the growth rate. It can be seen in Figure 3 that the growth rate is higher for the sample with a grain size of 0.5 µm, which proves the presence of a high K value. On the other hand, the nucleation sites for other samples are the shear band intersections, and hence, it is logical that they follow the same trend.

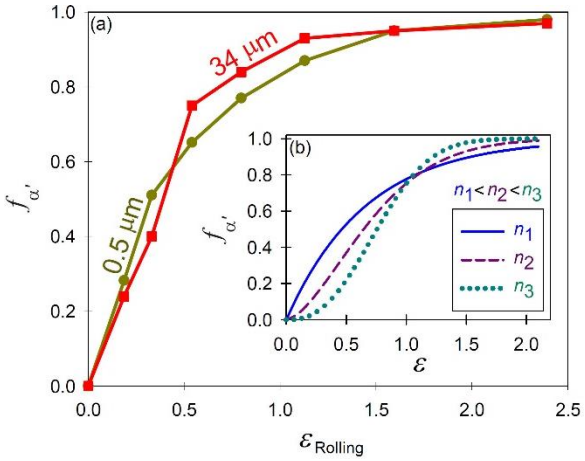

Fig. 7. (a) Martensite content versus the cold rolling equivalent strain for grain sizes of 0.5 and 34 µm and (b) schematic representation of the effect of n.

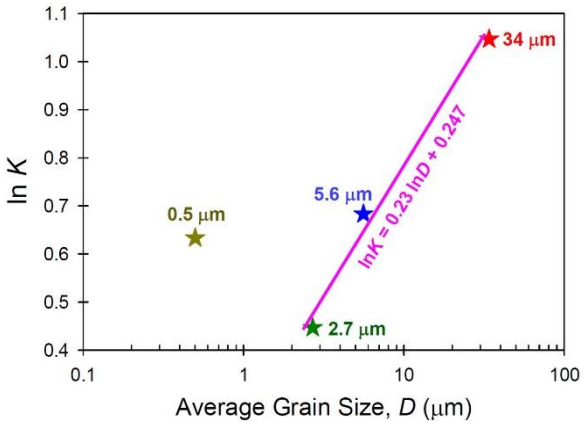

Fig. 8. lnK of JMAK-type analysis versus grain size.

4. CONCLUSIONS

The JMAK-type model was implemented for comparing the kinetics of α'-martensite formation for the UFG and coarse-grained regimes using an AISI 304L stainless steel accompanied by an experimental investigation. The following conclusions can be drawn:

1) By considering the dependency of the volume fraction of α'-martensite on the strain, the JMAK-type model was found to be a useful tool for modelling the experimental data, predicting the nucleation sites based on the theoretical Avrami exponents, and characterizing the transformation kinetics at low and high strains.
2) JMAK-type analysis for the UFG sample resulted in an *n* value of ~1 but for other samples, the value of ~1.6 was obtained. The former is related to the nucleation on grain boundaries (α'-martensite directly formed from austenite), which was verified by EBSD analysis as well as for another stainless steel based on the literature data.

REFERENCES

[1]. Zhou, Z., Wang, S., Li, J., Li, Y., Wu, X. and Zhu, Y., "Hardening after annealing in nanostructured 316L stainless steel." Nano Mater. Sci., 2020, 2.1, 80-82.

[2]. Somani, M.C., Jaskari, M., Sadeghpour, S., Hu, C., Misra, R.D.K., Nyo, T.T., Yang, C. and Karjalainen, L.P., "Improving the yield strength of an antibacterial 304Cu austenitic stainless steel by the reversion treatment." Mater. Sci. Eng. A, 2020, 793, 139885.

[3]. Khorrami, M., Zarei-Hanzaki, A., Abedi, H.R., Mola, J., Chen, G. and Minarik, P., "Temperature dependence of tensile deformation behavior and strain hardening of lean duplex stainless steels." J. Mater. Res. Technol., 2022, 20, 330-342.

[4]. Sohrabi, M.J., Mirzadeh, H., Sadeghpour, S. and Mahmudi, R., "Explaining the drop of work-hardening rate and limitation of transformation-induced plasticity effect in metastable stainless steels during tensile deformation." Scr. Mater., 2023, 231, 115465.

[5]. Qin, W., Li, J., Liu, Y., Kang, J., Zhu, L., Shu, D., Peng, P., She, D., Meng, D. and Li, Y., "Effects of grain size on tensile property and fracture morphology of 316L stainless steel." Mater. Lett., 2019, 254, 116-119.

[6]. Shirdel, M., Mirzadeh, H. and Parsa, M.H., "Nano/ultrafine-grained austenitic stainless steel through the formation and reversion of deformation-induced martensite: Mechanisms, microstructures, mechanical properties, and TRIP effect." Mater. Charact., 2015, 103, pp.150-161.

[DOI: 10.22068/ijmse.3335]

[7]. Sohrabi, M.J., Mirzadeh, H., Sadeghpour, S., Mahmudi, R., "Grain size-dependent mechanical behavior and TRIP effect in a metastable austenitic stainless steel." Int. J. Plast., 2023, 160, 103502.
[8]. Huang, M., Wang, L., Wang, C., Mogucheva, A. and Xu, W., "Characterization of deformation-induced martensite with various AGSs upon Charpy impact loading and correlation with transformation mechanisms." Mater. Charact., 2022, 184, 111704.
[9]. Eskandari, M., Zarei-Hanzaki, A. and Abedi, H.R., "An investigation into the room temperature mechanical properties of nanocrystalline austenitic stainless steels." Mater. Des., 2013, 45, 674-681.
[10]. Huang, M., Yuan, J., Wang, J., Wang, L., Mogucheva, A. and Xu, W., "Role of martensitic transformation sequences on deformation-induced martensitic transformation at high strain rates: A quasi in-situ study." Mater. Sci. Eng. A, 2022, 831, 142319.
[11]. Kishore, K., Kumar, R.G. and Chandan, A.K., "Critical assessment of the strain-rate dependent work hardening behaviour of AISI 304 stainless steel." Mater. Sci. Eng. A, 2021, 803, 140675.
[12]. Kisko, A., Misra, R.D.K., Talonen, J. and Karjalainen, L.P., "The influence of grain size on the strain-induced martensite formation in tensile straining of an austenitic 15Cr–9Mn–Ni–Cu stainless steel." Mater. Sci. Eng. A, 2013, 578, 408-416.
[13]. Sun, G., Zhao, M., Du, L. and Wu, H., "Significant effects of grain size on mechanical response characteristics and deformation mechanisms of metastable austenitic stainless steel." Mater. Charact., 2022, 184, 111674.
[14]. Naghizadeh, M. and Mirzadeh, H., "Modeling the kinetics of deformation-induced martensitic transformation in AISI 316 metastable austenitic stainless steel." Vacuum, 2018, 157, 243-248.
[15]. Olson, G.B. and Cohen, M., "Kinetics of strain-induced martensitic nucleation." Metall. Mater. Trans. A, 1975, 6, 791-795.
[16]. Ahmedabadi, P.M., Kain, V. and Agrawal, A., "Modelling kinetics of strain-induced martensite transformation during plastic deformation of austenitic stainless steel." Mater. Des., 2016, 109, 466-475.
[17]. Tavares, S.S.M., Pardal, J.M., Da Silva, M.G., Abreu, H.F.G.D. and da Silva, C.R., "Deformation induced martensitic transformation in a 201 modified austenitic stainless steel." Mater. Charact., 2009, 60(8), 907-911.
[18]. Zheng, C., Jiang, H., Hao, X., Ye, J., Li, L. and Li, D., "Tailoring mechanical behavior of a fine-grained metastable austenitic stainless steel by pre-straining." Mater. Sci. Eng. A, 2019, 746, 332-340.
[19]. Shin, H.C., Ha, T.K. and Chang, Y.W., "Kinetics of deformation-induced martensitic transformation in a 304 stainless steel." Scr. Mater., 2001, 45(7), 823-829.
[20]. Mansourinejad, M. and Ketabchi, M., "Modification of Olson–Cohen model for predicting stress-state dependency of martensitic transformation." Mater. Sci. Technol., 2017, 33(16), 1948-1954.
[21]. Sohrabi, M.J., Mirzadeh, H., Sadeghpour, S. and Mahmudi, R., "Dependency of work-hardening behavior of a metastable austenitic stainless steel on the nucleation site of deformation-induced martensite." Mater. Sci. Eng. A, 2023, 868, 144600.
[22]. Naghizadeh, M. and Mirzadeh, H., "Microstructural evolutions during reversion annealing of cold-rolled AISI 316 austenitic stainless steel." Metall. Mater. Trans. A, 2018, 49, 2248-2256.
[23]. Shirzad, K. and Viney, C., "A critical review on applications of the Avrami equation beyond materials science." J. R. Soc. Interface., 2023, 20(203), 20230242.
[24]. Rafiei, M., Mirzadeh, H., Malekan, M. and Sohrabi, M.J., "Homogenization kinetics of a typical nickel-based superalloy." Journal of Alloys and Compounds, 2019, 793, pp.277-282.
[25]. Mirzadeh, H. and Najafizadeh, A., "Extrapolation of flow curves at hot working conditions." Mater. Sci. Eng. A, 2010, 527(7-8), 1856-1860.
[26]. Malekan, M., Rashidi, R. and Shabestari, S.G., "Mechanical properties and crystallization kinetics of Er-containing Cu–Zr–Al bulk metallic glasses with

[DOI: 10.22068/ijmse.3335]

excellent glass forming ability." Vacuum, 2023, 174, 109223.
[27]. Ghaemifar, S. and Mirzadeh, H., "Dissolution kinetics of Laves phase during homogenization heat treatment of additively manufactured Inconel 718 superalloy." J. Matter, Res. Technol., 2023, 24, 3491-3501.
[28]. Alhaji, A., Razavi, R.S., Ghasemi, A. and Loghman-Estark, M.R., "Crystallization kinetics of $MgO–Y_2O_3$ composite nanopowder synthesized via combustion sol–gel method." J. Therm. Anal. Calorim., 2018, 132, pp.1325-1332.
[29]. Nasiri, Z., Ghaemifar, S., Naghizadeh, M. and Mirzadeh, H., "Thermal mechanisms of grain refinement in steels: a review." Met. Mater. Int., 2021, 27, 2078-2094.
[30]. Abdi, A., Mirzadeh, H., Sohrabi, M.J. and Naghizadeh, M., "Phase transformation kinetics during annealing of cold-rolled AISI 309Si stainless steel." Metall. Mater. Trans. A, 2020, 51, 1955-1959.

[DOI: 10.22068/ijmse.3335]